NPL
National Physical Laboratory

NPL REPORT
DEPC MPE 019

Preparation and characterisation of PEM fuel cell electrocatalysts: a review

G. HINDS

NOT RESTRICTED

OCTOBER 2005

dti
FUNDED BY THE DTI

National Physical Laboratory | Hampton Road | Teddington | Middlesex | United Kingdom | TW11 0LW
Switchboard 020 8977 3222 | **NPL Helpline** 020 8943 6880 | **Fax** 020 8943 6458 | **www.npl.co.uk**

Preparation and characterisation of PEM fuel cell electrocatalysts: a review

G. Hinds
DEPC

ABSTRACT

A critical review of the literature has been undertaken to summarise current techniques for the preparation and characterisation of polymer electrolyte membrane (PEM) fuel cell catalysts. Both catalyst particle and electrode preparation techniques are considered. Key measurement issues are identified in the context of the Materials Programmes.

ISSN 1744-0262

National Physical Laboratory
Hampton Road, Teddington, Middlesex, TW11 0LW

Approved on behalf of the Managing Director, NPL
By Dr M G Gee, Knowledge Leader, DEPC

CONTENTS

1. INTRODUCTION

Fuel cells are promising candidates as environmentally friendly power sources for stationary, portable and automotive applications. The advantages of fuel cells over other sources of power are high efficiency, low emissions, modularity, fuel flexibility and high power density. The high efficiency arises from the fact that fuel cells convert chemical energy directly to electrical energy without the Carnot limitation that applies to thermal engines. The efficiency of fuel cells for generating electricity is 40%–60% and can reach 85%–90% in combined heat and power (CHP) mode, i.e. if the heat generated from the cell reaction is also used. The only waste product is pure water when hydrogen is used as the fuel. Fuel cells can be used on a micro/local level without loss of efficiency, thereby avoiding transmission losses associated with long distance power lines. The three major issues currently confronting fuel cell developers and manufacturers are cost of components, establishment of a refuelling infrastructure and durability of the systems in service.

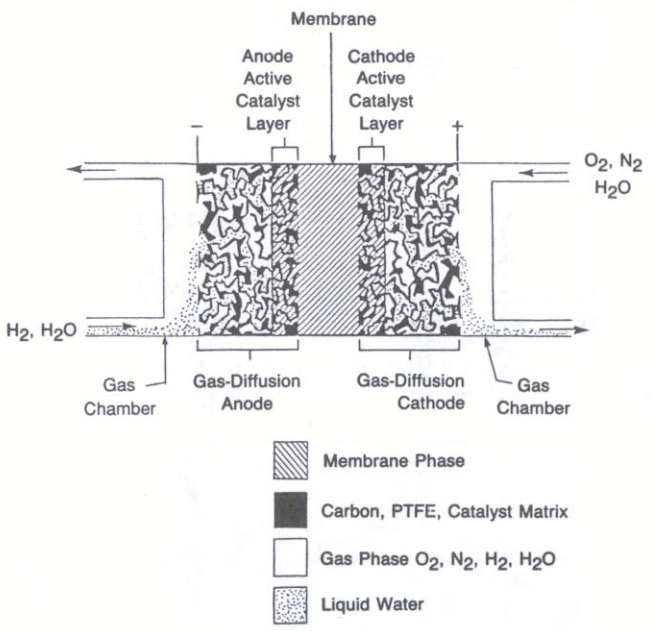

Figure 1.1 Components of a PEMFC[1].

The polymer electrolyte membrane fuel cell (PEMFC) is considered the most likely candidate for transport applications due to its high power density, low operating temperature (for fast start-up), high power-to-weight ratio and absence of corrosive fluids. The technology was initially developed by General Electric in the 1960s for use by NASA on their first manned space missions. The Gemini program employed a 1 kW PEMFC stack as an auxiliary power source that also provided the astronauts with clean drinking water. The electrolyte membrane was a polystyrene sulphonate polymer that proved unstable, prompting NASA to switch to alkaline fuel cell technology for subsequent missions. In the late 1980s Ballard Power Systems (Vancouver) and Los Alamos National Labs (California) began developing PEM fuel

cells with a Nafion membrane manufactured by Dupont, which is more stable than the polystyrene sulphonate polymer. The next decade saw a dramatic decrease in catalyst loading and substantially improved performance. Increased funding from the automotive sector and energy policy promoting fuel cells have positioned PEMFC cell technology on the brink of widespread commercial uptake, with most manufacturers well into the demonstration stage and some already operating in niche markets.

The various components of a PEMFC are shown schematically in Figure 1.1. The fuel is supplied to the anode and the oxidant (oxygen or air) to the cathode. Hydrogen is the most common fuel, although methanol is used in a variant of the PEMFC known as the direct methanol fuel cell (DMFC)[2]. In a H_2/O_2 cell, the following reaction occurs at the anode:

$$H_2 \rightarrow 2H^+ + 2e^- \tag{1}$$

The dissociation of H_2 and adsorption of hydrogen atoms on the anode catalyst leads to the formation of H^+ ions, which migrate to the cathode through the proton-conducting membrane. Since the membrane is electronically insulating, the electrons are forced to flow through an external load to the cathode, thereby generating dc current. At the cathode H^+ ions, electrons and oxygen molecules combine to form water in the following reaction:

$$O_2 + 4H^+ + 4e^- \rightarrow 2H_2O \tag{2}$$

The stoichiometry of each reactant gas is an important experimental parameter in fuel cell testing. A 1:1 stoichiometry refers to the flow rate required to maintain a constant reactant concentration at the electrode at a fixed current density (reaction rate). Usually a higher stoichiometry is required at the cathode (typically 2-4) than at the anode (typically 1-2) due to the more sluggish mass transport rate of oxygen. This should not be confused with the fact that two moles of hydrogen are required for every mole of oxygen taking part in the reaction. The water produced in the cathodic reaction is removed by the excess gas stream and flooding can occur if the gas flow rate and temperature are not sufficiently high.

The properties of the solid polymer membrane at the heart of the PEMFC are critical to its operation. Nafion is the most common membrane employed at present, although novel membranes are currently the subject of considerable research effort. Nafion is a derivative of PTFE, which consists of a hydrophobic PTFE backbone with hydrophilic sulphonic acid side chains. When these side chains are hydrated, the membrane can conduct protons while remaining electronically insulating, which is key to its use in PEM fuel cells. Nafion is a translucent plastic material, which is resistant to chemical attack, a strong proton donor, transports water rapidly and can function as both a super-acid catalyst and a cation exchange membrane. Its conductivity is highly dependent on water content, which means that water management is an essential part of PEMFC operation. This is normally achieved by humidification of inlet gases. Due to the requirement for Nafion to be hydrated,

membrane use is limited to below 100 °C at ambient pressure. Research into higher temperature membranes is an important developmental step in PEMFC technology. A Dow membrane also based on sulphonated PTFE but with shorter side chains and improved transport properties was developed in the 1980s. The power density achievable using this membrane was more than double that of Nafion. However most research groups continue to use Nafion due to its lower cost and ease of membrane fabrication.

On each side of the membrane is a thin layer of nanoparticulate precious metal catalyst of order 10 μm in thickness. The catalyst may be either unsupported as a nanoparticulate powder or supported on high surface area graphitic carbons (200 m^2 g^{-1}). Supported catalysts are typically 20-40 wt% metal with catalyst loadings in the range 0.1-0.5 mg cm^{-2}. Due to the low operating temperature and acidic environment, precious metal catalysts are required. Platinum is the most effective catalyst known for both oxidation of hydrogen and reduction of oxygen reactions. However, the activity of platinum catalysts may be severely reduced by small concentrations (> 10 ppm) of carbon monoxide (CO) in the reactant gas. This is of particular concern for systems using reformate (hydrogen processed from natural gas). For this reason the anode catalyst is often a PtRu alloy, which is more resistant to carbon monoxide poisoning.

The reactant gas is fed to each electrode through a gas diffusion layer (GDL), which is typically made from carbon cloth or carbon paper. The dual function of the GDL is (a) to allow reactant gas to diffuse uniformly to the catalyst layers and (b) to collect current from reaction sites. In addition, a hydrophobic phase (usually PTFE) is often added to the GDL to avoid flooding. It follows that candidate materials for the GDL must have high porosity, low resistance and low cost. The GDL must also be able to withstand compressive forces and chemical attack. The membrane together with catalyst and backing layers is known as a membrane electrode assembly (MEA).

The Three Phase Boundary (TPB) is a zone in which the open pores, catalyst and electrolyte are in close contact. The reaction process requires flow of protons via the electrolyte, supply of reactant gas through open pores and flow of electrons in the GDL. The active layer therefore contains an intimate mixture of electrolyte and catalyst, with intermingled electronic, ionic and mass transport pathways. Diffusion of reactant through electrolyte is a significant source of mass transport limitation. The detailed mechanisms of charge transport, mass transport and electrocatalytic reaction within the TPB are not well understood.

This review summarises the common methods employed in the preparation and characterisation of both Pt/C catalysts and PEMFC electrodes. Key measurement issues are identified in the context of the Materials Programmes. For simplicity, the discussion of catalyst materials is largely confined to Pt, which remains the most suitable catalyst for low temperature fuel cells. Due to its relatively high cost, the search continues for cheaper alternatives, for which a compromise between cost and performance is necessary.

2. CATALYST PREPARATION AND CHARACTERISATION

The industry standard for PEM fuel cell catalysts is highly dispersed nanocrystalline platinum on a carbon support (Pt/C), as shown in Figure 2.1. The small darker particles are Pt (typical diameter 2-3 nm) and the larger particles are carbon (typically 30 nm in size). These catalysts have a high exchange current density for both hydrogen oxidation and oxygen reduction. PtRu is commonly used at the anode due to its higher tolerance to carbon monoxide (CO) poisoning. A range of catalysts is commercially available from companies such as E-TEK and Vulcan. These catalysts are typically prepared in three steps:

1. Dispersion of Pt on support
2. Reduction of Pt
3. Thermal activation

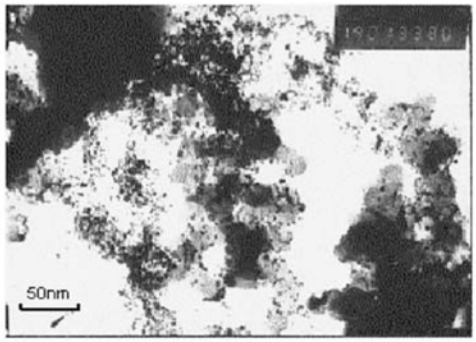

Figure 2.1 TEM micrograph of Pt/C catalyst[3].

The choice of support is critical to the catalytic properties. Auer et al[4] have reviewed the physical and chemical properties of carbon support materials, while various preparation techniques have been recently reviewed by Antolini[5]. Activated carbon is usually employed, although research is now increasingly being directed towards other forms of carbon, e.g. nanotubes. Dispersion of Pt on the carbon support is typically carried out by either impregnation or colloidal methods, which are described below. A reduction step is then carried out, as outlined in Section 2.3. Finally, the catalyst is thermally activated by heat treatment in an inert atmosphere (see Section 2.4). The impregnation method is used to obtain a uniform distribution of platinum throughout the particles of the carbon support. Here, diffusion of the hexachloroplatinic anion into the pores of the support material is possible due to the equilibrium between adsorbed and free ions. The colloidal method yields a core-shell distribution, due to the larger size of the colloid particles.

Characterisation of catalytic material is usually carried out using a combination of imaging techniques (SEM, TEM) and structural/chemical analysis (XRD, XPS). For electrochemical characterisation, the catalyst is either incorporated into a half-cell configuration or a full MEA.

2.1 DISPERSION STEP

Impregnation method

The carbon support is impregnated with an aqueous solution of hexachloroplatinic acid (H_2PtCl_6) in acid media, or tetra-amine platinum chloride [$Pt(NH_3)_4Cl_2$] in basic media. Czaran et al[6] showed that after impregnation and drying in air, the platinum was present as Pt^0 and Pt^{2+}, implying that a redox process had occurred. Miguel et al[7] studied the impregnation step using XPS and concluded that the metal complex is stabilised as Pt^{2+} on the carbon surface. They found no effect of carbon surface chemistry on the resulting oxidation state of Pt. The presence of Pt^{2+} following impregnation was confirmed by other authors[8,9]. Analysis of adsorption isotherms revealed non-Langmuir type behaviour[10,11], with both strong and weak adsorption of platinum. Van Dam and van Bekkum[23] proposed a model to describe the impregnation step, whereby the carbon reduces the Pt(IV) complex to a Pt(II) complex, which is then anchored to the support via a ligand site.

The issue of ligand sites has been a matter of debate in the literature. It is generally accepted that carbon surface basic sites act as strong anchoring sites for the hexachloroplatinic anion. These surface basic sites are associated with π-electron rich regions in the basal planes[12]. Leon et al[13] postulated that protonation of such sites leads to the following equilibrium:

$$C_\pi + H_3O^+ \leftrightarrow [C_\pi–H_3O]^+ \tag{2.1}$$

$$C_\pi + 2H_2O \leftrightarrow [C_\pi–H_3O]^+ + OH^- \tag{2.2}$$

where C_π is a graphitised carbon surface platelet with partial localisation of lone π-electron pairs. Acidic oxygen surface groups on the carbon ($[C_\pi–H_3O]^+$) act as weak anchoring sites. Lambert and Che[14] proposed an improved model for the strong adsorption of platinum, whereby surface groups replace the original ligands of the metal complex. This could occur without simultaneous reduction by the insertion of a water ligand:

$$Pt(IV)Cl_6^{2-} + [C_\pi–OH_3]^+ \leftrightarrow [C–OH_2–Pt(IV)Cl_5]^- + HCl \tag{2.3}$$

or with simultaneous reduction to Pt(II):

$$Pt(IV)Cl_6^{2-} + [C_\pi–OH_3]^+ \leftrightarrow [C–O–Pt(II)Cl_3]^- + 3HCl \tag{2.4}$$

Experimental support for this mechanism was provided by Fourier transform extended X-ray absorption fine structure (FT-EXAFS) analysis of Pt/C catalysts prepared by the impregnation method[15], which showed that the strong interaction between the Pt complex and the carbon support was associated with the change in Pt coordination from chlorine to oxygen atoms. Ageeva et al[16] demonstrated that ultraviolet (UV) radiation affects the rate of adsorption of platinum on activated carbon, but has no effect on the thermodynamics of the process.

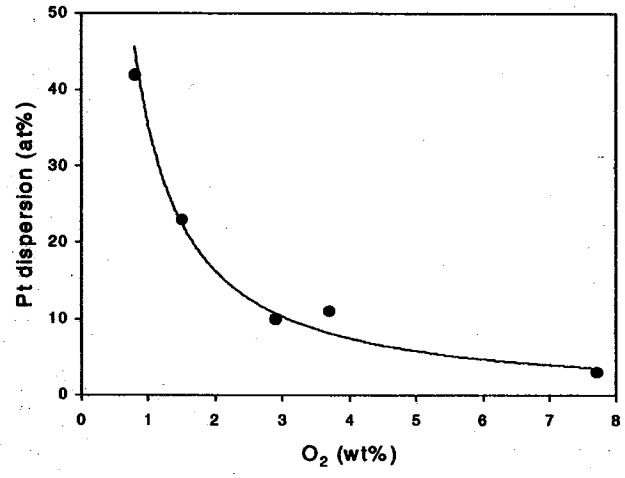

Figure 2.2 Effect of surface oxygen concentration of carbon support on Pt dispersion in Pt/C catalysts[17].

The carbon surface is often pre-treated with oxidising agents such as nitric acid (HNO_3), hydrogen peroxide (H_2O_2), oxygen (O_2) or ozone (O_3). This pre-treatment destroys surface basic sites and forms surface acidic sites. Contradictory reports as to the effect of oxygen surface groups on the dispersion of Pt may be found in the literature. Torres et al[18] compared the effect of different oxidising agents on the nature of the functional groups on the treated surface. They found that HNO_3-treated carbon had a high density of strong and weak acidic sites, while the H_2O_2- and O_3-treated carbon had a higher proportion of weak acidic sites. The less acidic sites showed a stronger interaction with the platinum precursor. They reported an increase in Pt dispersion with increasing density of oxygen surface sites, which was supported by other authors[19,20]. Sepulveda et al[21] showed a similar increase in Pt dispersion in the presence of oxygen surface groups with $Pt(NH_3)_4Cl_2$ as precursor but no effect with H_2PtCl_6. However, some authors report a decrease in catalyst dispersion in the presence of oxygen surface groups[22,23]. Guerrero-Ruiz et al[24] showed using microcalorimetry of carbon monoxide (CO) adsorption that the metal-support interaction was weakened by the presence of oxygen surface groups. A similar observation was made by Fraga et al[25], who showed that the Pt dispersion decreased with surface oxygen concentration on the support as shown in Figure 2.2. The authors attributed this decrease to a reduction in the number of surface basic sites, where strong adsorption of $PtCl_6^{2-}$ takes place.

Research into alternative forms of carbon has increased in recent years. Yuan et al[26] prepared platinum catalyst particles supported on a variety of carbon nanotubes (CNTs) and carbon nanofibres (CNFs) by the impregnation method. A better performance was obtained with the shorter twisted CNFs than with either the longer twisted CNFs, straight CNFs or CNTs. The higher performance of the twisted CNFs was attributed to the enhanced metal-support interaction in that particular configuration. Liu et al[27] also prepared Pt/C nanotube catalysts, for which XPS analysis revealed a composition of 67.3% Pt^0 and 32.7% Pt^{4+}. Moreira et al

investigated the properties of Pd/C and Pd/Vulcan catalysts prepared by the impregnation method and found that the Pd/Vulcan showed a better performance.

Colloidal method

The colloidal method for producing Pt/C catalysts consists of the preparation of a Pt metal colloid followed by adsorption onto the carbon support. Alternatively, a Pt oxide colloid may be prepared; in this case the adsorption and reduction steps can take place either simultaneously or consecutively depending on the method used. The most common colloidal preparation techniques are the sulfite-complex and alcohol reduction methods.

In the sulfite-complex technique, Pt sulfite complexes are prepared from aqueous solutions of H_2PtCl_6 and $NaHSO_3$ containing suspended carbon support particles. A simultaneous oxidative decomposition and adsorption of the complex is induced by addition of H_2O_2. Antolini et al[28] used transmission electron microscopy (TEM) to characterise the particle size distribution of 20% Pt/C catalyst prepared by E-TEK using this method and found a monomodal distribution in the range 1.2 – 4.3 nm with a mean particle size of 2.6 nm. Uchida et al[29] investigated the effect of specific surface area of different carbon supports on the mean Pt particle size of catalysts prepared by the sulfite-complex method. The Pt particle size decreased with increasing specific surface area of the carbon support, as shown in Figure 2.3. A similar trend was observed by Watanabe et al[30]. This was rationalised by the fact that as the specific surface area of the carbon support decreases, more colloid particles are adsorbed on Pt particles rather than on the carbon support. The trend is in contrast to that observed for catalysts prepared by the impregnation method, where no significant effect of specific surface area of carbon support on Pt particle size was observed[31].

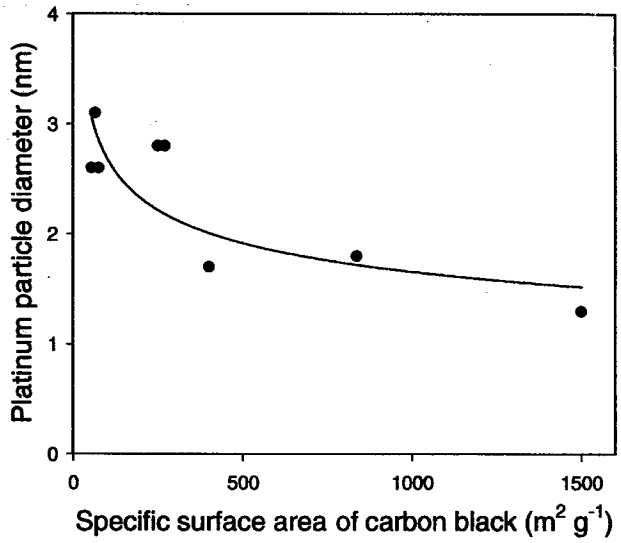

Figure 2.3 Effect of specific surface area of carbon support on mean Pt particle size[32].

In the alcohol reduction method, a suspension of H_2PtCl_6 and carbon support particles is reduced with methyl alcohol in the presence of a surfactant. The reaction is usually carried out in the temperature range 60-80 °C with stirring of the suspension to assist mass transport. Honji et al[33] studied the effect of surfactant concentration on Pt particle size, using sorbitan monolaurate as the surfactant. The Pt particle size decreased with increasing concentration of surfactant, with a more pronounced effect following heat treatment, as shown in Figure 2.4. Wang and Hsing[34] found that Pt particle size decreased with synthesis temperature when using dodecyldimethyl (3-sulfopropyl) ammonium hydroxide as surfactant (see Figure 2.5).

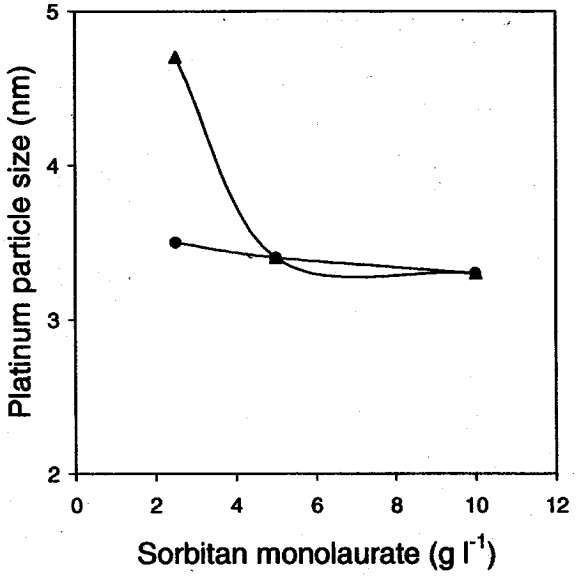

Figure 2.4 Effect of sorbitan monolaurate concentration on mean Pt particle size before (•) and after (▲) heat treatment[35].

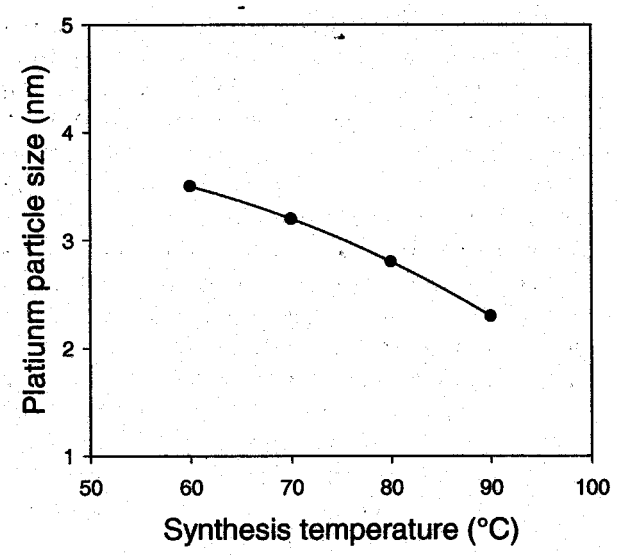

Figure 2.5 Effect of synthesis temperature on mean Pt particle size[36].

Like the impregnation method, the colloidal method has recently been used to produce platinum dispersions on a range of novel supports. Yoshitake et al[37] synthesised platinum catalyst particles supported on carbon nanohorns using the colloidal method. They obtained a uniform dispersion with a mean particle size of around 2 nm. Kim et al[38] prepared Pt catalyst particles supported on mesoporous carbon using mesoporous silica as a template.

The development of binary and ternary alloy catalysts by the colloidal method has attracted interest in recent years. Franco et al[39] prepared Pt-Ru-Mo catalyst particles on Vulcan XC-72 via the reduction of $PtCl_2$, $RuCl_3$ and $MoCl_5$.

2.2 REDUCTION STEP

Reduction of Pt following the impregnation or adsorption step can be carried out in a number of different ways. The catalyst may be dried and then heated in flowing H_2 in the temperature range 300 °C – 500 °C or a reducing agent may be added directly to the colloidal suspension. Common reducing agents are sodium borohydride ($NaBH_4$), sodium sulphite ($Na_2S_2O_4$) and nitrogen hydride (N_2H_2). Alternatively, the reduction step may be performed electrochemically using H_2SO_4 as the electrolyte. The reduction of Pt is never complete and some oxide species remain on the carbon support following the treatment. Nucleation and growth of Pt particles occurs during this step.

The effect of preparation conditions during the reduction step was investigated by Tian et al[40]. They found that the mean Pt particle size was dependent on the temperature and on the nature of the reducing agent. The mean Pt particle size decreased with decreasing strength of the reducing agent, which was attributed to increased adsorption of $PtCl_6^-$ anions on the carbon surface. The mean Pt particle size was found to increase with temperature. This was explained by a simple nucleation and growth model, whereby as the temperature is increased particle growth is enhanced and nucleation is suppressed.

Stoyonova et al[41] showed that the reduction method affects the nature of the crystal faces exposed at the particle surface, as well as the particle size and extent of oxidation of the carbon support. Antolini et al[42] highlighted the role of sulphur from decomposition of $Na_2S_2O_4$ in providing sites for nucleation and growth of Pt particles. The decomposition in acid media proceeds as follows:

$$S_2O_4^{2-} + 2H^+ \rightarrow H_2S_2O_4 \rightarrow S + H_2SO_4 \qquad (2.5)$$

forming finely divided sulphur particles, which serve as nucleation sites for Pt particles, depending on the characteristics of the carbon support. For weak metal-support interactions, observed with Vulcan XC-72R carbon in the impregnation method, growth of small Pt crystallites on sulphur particles is favoured due to the high number of sulphur particles and a high Pt dispersion is obtained. The opposite occurs with Ketjen-black type carbons, where the strong metal-support interaction at surface

basic sites dominates and nucleation occurs preferentially at these sites[43]. In this case the growth of a smaller number of larger particles is favoured.

2.3 THERMAL ACTIVATION

Thermal activation of the catalyst is carried out after the reduction step. This usually consists of a heat treatment under an inert atmosphere (nitrogen or argon) at a temperature in the range 80 °C – 900 °C. The duration of the heat treatment can be up to several hours. The aim of the activation step is to produce a uniform dispersion with a stable distribution of Pt particle size on the carbon support and to remove any undesirable impurities from the preparation process. Jalan et al[44] carried out heat treatment of Pt/C catalysts at 900 °C in a nitrogen atmosphere and observed growth from a broad distribution of Pt particles sizes in the range 1.5 – 3.5 nm to a more uniform normal distribution with a mean of 4.2 ± 0.5 nm. The particles were also more uniformly dispersed on the support following the heat treatment. Antolini et al[45] investigated the effect of thermal activation temperature on the mean Pt particle size for a Pt/Vulcan XC-72R catalyst prepared with $Na_2S_2O_2$ as reducing agent. They showed that sintering of Pt occurs in the range 300 °C – 400 °C, as shown in Figure 2.6, and concluded that the presence of sulphur enables Pt to move on the carbon surface by a bridge-bonding mechanism[46]. Torre et al[47] proposed that surface acidic groups act as anchoring sites for the Pt particles, thereby limiting their growth at lower temperatures.

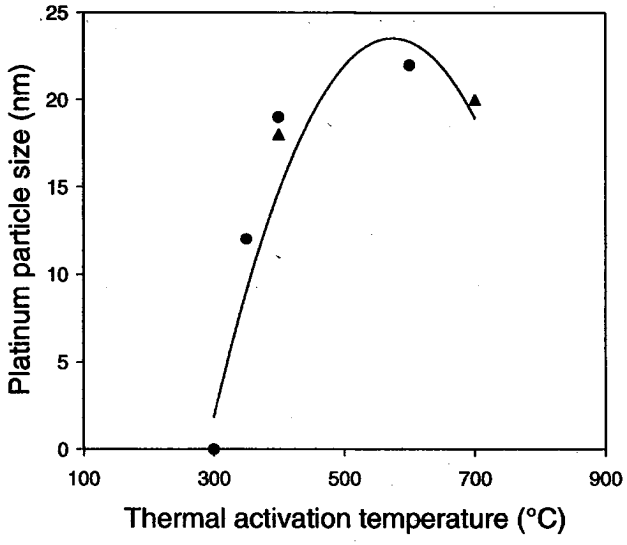

Figure 2.6 Effect of thermal activation temperature on mean Pt particle size from XRD (●) and TEM (▲) measurements on Pt/C catalysts[48].

2.4 CHARACTERISATION TECHNIQUES

Imaging techniques such as SEM and TEM are employed to characterise Pt/C catalysts on the micro- to nanoscale respectively. TEM is used to characterise the particle size and distribution of the catalyst and support. A typical catalyst consists of platinum particles of 2-3 nm in diameter, supported on agglomerates of carbon particles of ~ 30 nm in size, as shown in the TEM micrograph in Figure 2.1. Both of these imaging techniques and their variants (HR-SEM and STEM) are therefore extremely useful in the systematic investigation of the correlation between material fabrication methods and cell performance. Atomic resolution scanning probe techniques such as atomic force microscopy (AFM) and scanning tunnelling microscopy (STM) have limited applicability to catalyst materials due to their inhomogeneity and high surface roughness.

For structural characterisation of Pt/C catalysts, X-ray diffraction (XRD) is commonly used. X-ray absorption near-edge structure (XANES) and extended X-ray absorption fine structure (EXAFS) may also be utilised to obtain structural and chemical information about these catalysts. Mukerjee et al[49] showed using XRD that carbon-supported Pt has a fcc structure similar to that of bulk Pt. They also demonstrated identical d-band structures for Pt/C and bulk Pt using XANES. EXAFS measurements revealed a shift in coordination from 12 (bulk Pt) to 9 (Pt/C), which was attributed to a particle size effect on the fraction of surface atoms on the <111> and <100> faces of the Pt particles[50]. Romanovski[51] proposed a cubo-octahedral structure in order to minimise the surface energy. This was confirmed by Sattler and Ross[52] using HRTEM and by Komiyama et al[53] using STM. The ideal cubo-octahedral structure consists of eight octahedral <111> and six cubic <100> faces bounded by edge and corner atoms. In practice, a mixture of these and other faces is obtained. The normalised surface distribution of Pt atoms is plotted as a function of particle size in Figure 2.7, showing that the relative amount of edge and corner atoms is highest at low particle sizes.

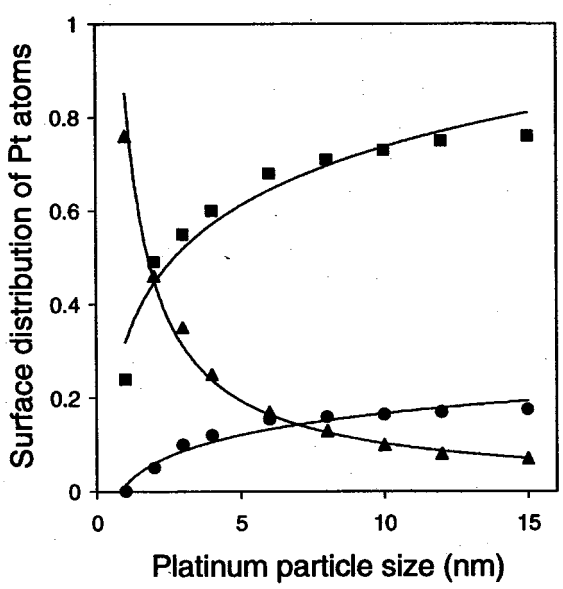

Figure 2.7 Surface distribution of Pt atoms as a function of particle size: <100> atoms (●),<111> atoms (■) and edge/corner atoms (▲)[54].

While Pt particle size is well documented, the issue of particle shape does not seem to have been widely addressed in the literature. It is often not clear when particle diameters are quoted whether this refers to spherical, flat or elongated particles. The shape of Pt particles has important consequences in terms of catalyst loading and performance.

3. ELECTRODE PREPARATION AND CHARACTERISATION

Electrode preparation techniques have undergone continuous evolution since the 1960s thanks to technological advances and the development of novel materials. During this time the typical platinum loading has decreased by a factor of 100 and the development of ionomer-impregnated electrodes has increased the power density by extending the three dimensional reaction zone. Commercial electrode preparation techniques are highly proprietary but the fundamental methods, together with those in the published literature, are reviewed here. In general terms, a PEMFC electrode consists of an intimate mixture of Pt/C catalyst (whose preparation is described in the previous section), ionomer and open pores, forming a three phase reaction zone. The charge and mass transport properties of the electrode and its diffusion layer(s) are critical to the performance of the fuel cell.

A summary of the evolution of typical preparation methods for PEMFC electrodes over the past decade or so is shown in Figure 3.1. The main features are the transition from two-layer to three-layer electrodes and the selection of different catalyst compositions for anode and cathode. Improvements in water management are reflected in the increased proportion of hydrophobic agent in the cathode diffusion layer relative to that of the anode.

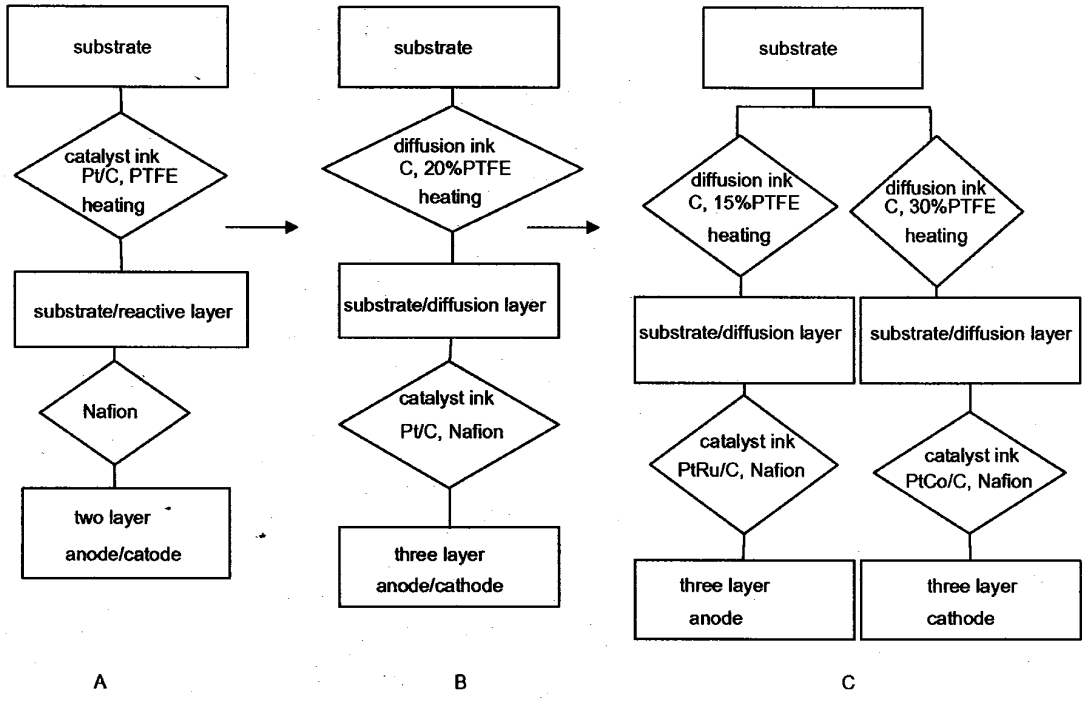

Figure 3.1 Evolution of typical preparation methods for PEMFC electrodes[55].

3.1 BILAYER ELECTRODES

A standard bilayer electrode consists of a carbon paper substrate and a porous catalyst layer. The properties of some commercially available carbon papers commonly used as substrates in PEMFC electrodes are listed in Table 3.1.

Table 3.1 Properties of commercially available carbon papers used as substrates in PEMFC electrodes[56].

Carbon paper	Thickness (mm)	Porosity (%)	Density (g cm^{-3})
Toray TGPH 090	0.30	77	0.45
Kureha E-715	0.35	60-80	0.35-0.40
Spectracarb 2050A-1040	0.25	60-90	0.40

The substrate is loaded with a hydrophobic agent such as fluoroethylenepropylene (FEP) or polytetrafluoroethylene (PTFE) in order to enhance transport of water away from the catalyst layer and prevent flooding. There is an optimum loading level, beyond which ohmic losses become significant and reaction sites are blocked by the polymer. Staiti et al[57] investigated the effect of FEP loading on the fuel cell performance and found a maximum at around 30 wt% FEP.

The catalyst layer typically consists of a mixture of Pt/C or Pt alloy/C, ionomer and PTFE. The ionomer provides a proton conducting path to increase the effective interface between the membrane and the catalyst. The PTFE serves as a hydrophobic agent. A suspension of catalyst, ionomer and PTFE (known as a catalyst ink) is applied directly onto the wet-proofed carbon paper. The solvent is typically an alcohol, such as isopropyl alcohol. A number of methods have been developed for the application of the ink, including spraying[58], brushing[59], screen printing[60], tape casting[61] and rolling[62]. Glycerol is often added to adjust the viscosity of the ink. Pore forming materials, e.g. ammonium salts, and sparingly soluble fillers such as lithium carbonate are added to adjust the fine and coarse porosities respectively[63]. The electrode is then dried in air and heat treated/sintered and the carbon paper is hot pressed onto the membrane[64,65]. Alternatively, the ink may be deposited directly onto the membrane[66,67] or indirectly via a decal from which the electrode is transferred to the membrane by hot pressing[68,69].

From a mass transport perspective, the porosity of the catalyst layer is of critical importance to the operation of the fuel cell. If the thickness and composition of the catalyst layer are known, the porosity can be calculated simply by dividing the volume of the solid phase by the total volume of the electrode. Otherwise, the porosity can be determined by filling the pore structure with an inert solvent such as toluene[70]. Mercury or gas porosimetry are often used to characterise the pore size distribution of the catalyst layer. Mercury porosimetry is used to characterise larger pore sizes (3 nm – 300 μm), while nitrogen porosimetry is suited to smaller pore sizes in the range 0.5 nm – 100 nm. Relatively large volumes of sample are required, which often means that the sample has to be cut into small pieces and stacked in the sample holder. This perturbs the pore size distribution above 1 μm, making the quantitative determination

of porosity more difficult. For low pore sizes, the high pressure required may result in collapse of the pore structure[71].

Several groups have attempted to characterise the microstructure of the catalyst layer using mercury and gas porosimetry. Watanabe et al[72] characterised the pore structure of active layers consisting of a mixture of ionomer and Pt/C and found that there were two distinctive pore distributions with a boundary at around 0.1 μm. The primary (smaller) pore size was identified with the space between the particles in the agglomerate of the carbon support while the secondary pore size was identified with the space between the agglomerates. Uchida et al[73] later postulated that the ionomer and therefore the reaction sites were confined to the secondary pores. They examined the performance of single cells as a function of ionomer content in the active layer. The volume of the secondary pores (0.04 – 1 μm) decreased linearly with increasing ionomer content, while that of the primary pores (0.02 – 0.04 μm) remained unchanged, confirming that the ionomer was only present in the larger pores[74]. The primary pores therefore act as gas channels.

More recently Lundblad[75] showed that different fabrication procedures result in very different microstructures in the catalyst layer. He found that the distribution of ionomer in the catalyst layer was critically dependent on the mixing treatment of the catalyst ink. Solvents in which the ionomer is more soluble, such as ethanol or isopropanol, increase the wetability to carbon by decreasing the surface tension. In this work, the catalyst powder was mixed, using ultrasound, with a 5% Nafion solution in propanol, methanol and water, containing proprietary dispersant additives from DuPont Fluoroproducts Ltd. A more uniform distribution of ionomer was observed, even penetrating and/or encapsulating the small primary particles (30 nm) of the carbon support. Lundblad pointed out that the use of butyl acetate, in which the ionomer is less soluble, would explain the different ionomer distribution in the work of Uchida et al. Different pore structures require different electrochemical models in order to understand their performance.

Gamburzev and Appleby[76] investigated the effect of incorporating proprietary pore forming additives to the cathode catalyst-ionomer ink. An optimal amount of pore former (33 wt%) was identified for the MEAs studied, which yielded a performance of 340 mA/cm^2 on air at 0.7 V compared to 210 mA/cm^2 with no pore former.

The influence of Nafion content on the structure and performance of the cathode active layer was investigated by Gode et al[77]. The volume fraction of Nafion, Pt/C and open pores as a function of Nafion content is shown in Figure 3.2. The porosity does not vary much between 10 wt% and 30 wt% Nafion, but decreases dramatically at higher Nafion contents. Data obtained from impedance spectroscopy were analysed using an agglomerate model[78] developed by the authors, which showed that the model broke down above 45 wt% Nafion. This was interpreted as a blocking of the pores and a non-percolating Nafion system at high Nafion contents.

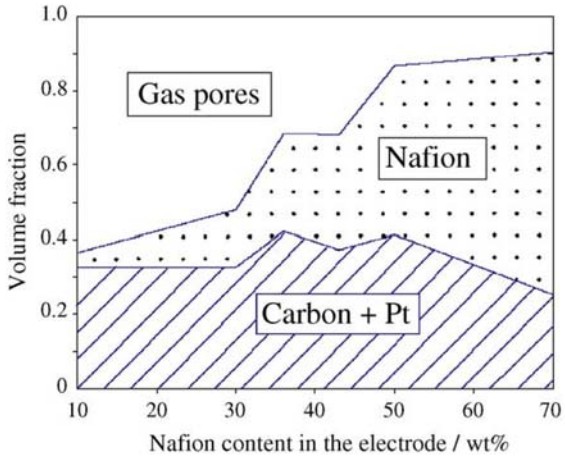

Figure 3.2: Volume fraction of gas pores, Nafion and Pt/C in an electrode as a function of Nafion content[79].

3.2 MULTILAYER ELECTRODES

The evolution of PEMFC electrodes towards a multilayer structure has been driven by advances in understanding of the fundamental processes occurring in the MEA. In the three layer electrode, a diffusion layer is inserted between the carbon paper and the catalyst layer. The diffusion layer consists of a mixture of carbon particles and PTFE and provides physical separation of the carbon paper from the catalyst layer, thereby reducing flooding and preventing catalyst particles from being trapped in the carbon paper when the MEA is under compression. It also provides a transition between the larger pore size of the carbon paper and the smaller pore size of the catalyst layer and prevents water condensed in the carbon paper from entering the catalyst layer. The PTFE in the diffusion layer acts both as a binder and a hydrophobic agent.

Preparation of three layer electrodes is essentially the same as that outlined above for bilayer electrodes, with an additional step for the diffusion layer. A suspension of carbon particles and PTFE is applied to the wet-proofed carbon paper, dried and thermally treated. The catalyst layer is then deposited onto the diffusion layer as described above to form the three layer electrode. Mass transport in the diffusion layer occurs in both the gaseous (reactant) and liquid (water) states, which requires a balance between hydrophilic (carbon) and hydrophobic (PTFE) pore surfaces. Lufrano et al[80] determined an optimum PTFE content in the diffusion layer of 20 wt% from polarisation measurements in a single H_2/air cell, while Song et al[81] obtained a higher value of 30 wt% using impedance spectroscopy. Antolini et al[82] reported that PTFE penetrates only the smaller pores between the carbon agglomerates (pore size < 1 μm). Above 40 wt% PTFE, they found that no further filling of pores occurs; instead the diffusion layer thickness increases.

Optimisation of diffusion layer characteristics should always be carried out at relatively high current densities, where mass transport is the limiting factor. For the same reason, such testing should be performed in H_2/air cells (rather than H_2/O_2 cells)

where the diluent effect of nitrogen shows up more clearly any differences in the efficiency of mass transport.

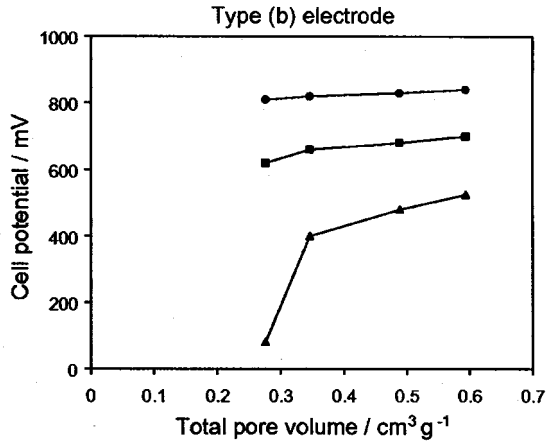

Figure 3.3 Cell potential as a function of total pore volume in the diffusion layer at 100 mA/cm^2 (•),400 mA/cm^2 (■) and 700 mA/cm^2 (▲)[83].

Passalacqua et al[84] investigated the effect of diffusion layer total pore volume on the fuel cell performance at a constant PTFE loading of 20 wt%. The total pore volume was varied by the use of different carbon particles in the diffusion layer. The cell potential at various current densities is plotted as a function of total pore volume in Figure 3.3. The performance increase with total pore volume is more dramatic at higher current densities, where mass transport effects are more significant. Kong et al[85] found that performance could be enhanced by incorporating macropores (50 – 100 μm) into the diffusion layer. The macropores absorb water from smaller pores, leaving them free to transport gas.

Since the reactions occurring at anode and cathode are very different, it follows that the diffusion layer structure and composition may be optimised in different ways for each electrode. Neergat and Shukla[86] demonstrated that cells with a more hydrophobic diffusion layer at the cathode and a more hydrophilic diffusion layer at the anode performed better than those with the same diffusion layer at both electrodes. In contrast, Moreira et al[87] found optimum PTFE contents of 10 wt% and 30 wt% for cathode and anode respectively. The reason for this discrepancy is not clear. Intuitively one might expect a more hydrophobic diffusion layer at the cathode since water is produced in the cathodic reaction.

When a diffusion layer is present, the incorporation of a hydrophobic agent in the catalyst layer is no longer necessary. The catalyst layer then consists of Pt/C and ionomer. It is desirable to achieve penetration of ionomer into the pore structure of the catalyst layer to provide an proton conducting path to the reaction sites. However, the ionomer coating on the pore walls should be as thin as possible to minimise the diffusion path for reactant gases. Various authors have studied the effect of ionomer content in the catalyst layer, using Nafion. As shown in Table 3.2, the optimum

Nafion loading in catalyst layers containing no PTFE (30-38 wt%) is higher than in PTFE-containing layers (25-27 wt%).

Table 3.2 Optimum Nafion loading in the catalyst layer.

Authors	PTFE used	Nafion loading (wt%)
Hsu et al[88]	Yes	25
Poltarewski et al[89]	Yes	27
Qi and Kaufman[90]	No	30
Li and Pickup[91]	No	30
Uchida et al[92]	No	33
Passalacqua et al[93]	No	33
Paganin et al[94]	No	35
Antolini et al[95]	No	38

Recent studies have shown that further improvements to electrode performance can be obtained by the use of carbon cloth with a diffusion layer on each side, i.e. one on the catalyst layer side and one on the gas side[96]. Antolini et al[97] claimed that the optimum combination for the cathode is a diffusion layer based on Vulcan carbon on the catalyst side and a diffusion layer based on Shawinigan carbon on the gas side.

The influence of the solvent used during the preparation process has been investigated by a number of authors. Kim et al[98] prepared catalyst inks using solvents of various polarities: isopropyl alcohol, methanol, dipropyl ketone (DPK) and n-butyl acetate (NBA). They found that the use of less polar solvents (DPK and NBA) led to a higher performance. This was attributed to a decrease in ionomer solubility, resulting in the formation of larger agglomerates. The dual benefit is an increase in proton conductivity and larger pore size for enhanced mass transfer. A similar study was carried out by Yang et al[99] using the following solvents: tetrabutylammonium hydroxide, NBA, iso-emyl alcohol, diethyl oxalate, ethylene glycol and ethylene glycol dimethyl ether. The performance of the electrodes was linked to the decomposition temperature of the solvent, of which ethylene glycol was found to be the most effective. The use of polyethylene oxide (PEO) was advocated by Abaoud et al[100]. Mustafa et al[101] demonstrated a correlation between agglomeration characteristic length in the suspension and pore diameter in the catalyst layer.

The drive to reduce Pt loading and increase catalyst utilisation has led to the development a range of novel preparation methods. Catalyst utilisation in MEAs prepared using standard techniques can be as low as 10%, mainly because the majority of Pt particles do not have access to proton conducting pathways (ionomer) or reactant gas (open pores). Loffler et al[102] prepared model electrodes by selective electrodeposition of Pt nanoparticles onto those areas of the carbon support that were in contact with the three phase boundary. They showed that pulsed electrodeposition was more effective in producing active catalysts. The advantage of this approach is that the majority of the Pt is located close to the surface and catalyst utilisation is increased, with inherent cost savings. A similar method was employed by Kim and Popov[103] to increase the catalyst loading near the surface to 75 wt% with a Pt loading of only 0.25 mg/cm^2 in a 5 μm thick catalyst layer. Hayashi et al[104] used

electrophoretic deposition to produce functionally graded electrode materials. An alternative approach proposed by Frey et al[105] was to fabricate the entire MEA (including the membrane) in a layer by layer approach by spraying or printing. This allows flexible control of layer thickness and composition and serial connection of individual cells during the fabrication process. Gulzow et al[106] have developed a dry powder fabrication technique involving rollers, which they claimed could be scaled up to a low cost, high throughput process. Foster et al[107] deposited conducting polymers as electronic pathways in electrodes with very low Pt loading thereby enhancing the catalyst utilisation. A preparation technique for electrodes using self-assembled Pt nanoparticles was developed by Pan et al[108].

The influence of porosity of the diffusion layer on PEMFC performance has been investigated by a number of authors. If the diffusion layer is too thick, ohmic and mass transfer losses will be too high, while if it is too thin the mechanical strength and contact resistance may be poor. Most of the effects of diffusion layer properties on fuel cell performance are observed at high current densities, where mass transport is the rate limiting factor. Prasanna et al[109] recently carried out a study of the effect of different commercial diffusion layers on the performance of single PEM fuel cells and concluded that gas permeability and pore diameter were the most important physical properties. They found that a mean pore size of above 60 μm results in greater losses at high current densities due to water droplet formation at the interface of the diffusion layer and the active layer. The gas permeability was severely affected by the hydrophobicity of the diffusion layer, which varies with PTFE content. The authors identified an optimum PTFE content of 20%. The influence of the porosity of the diffusion layer on cell performance was investigated by Chu et al using numerical simulation[110]. The results showed that a higher average porosity leads to a lower mass fraction of oxygen in the diffusion layer due to higher consumption of oxygen in the catalyst layer, meaning that a fuel cell designed to generate higher current will require a diffusion layer with a higher porosity. However, the simulations did not take into account flooding of the pores, which would limit the porosity level in practice.

3.3 ELECTROCHEMICAL CHARACTERISATION

The standard electrochemical technique for characterising the performance of both single cells and stacks is the measurement of potential as a function of current density under a set of constant operating conditions. The effect of composition, flow rate, temperature and relative humidity of the reactant gases may be varied systematically to investigate their effect on cell performance. An electronic load is used to dissipate the power generated in these experiments while maintaining the accuracy of the measurements. A plot of potential against current density is known as a polarisation curve and yields information about the losses in the cell or stack under service conditions. A typical polarisation curve for a single hydrogen/air fuel cell is shown in Figure 3.4. At low current densities the majority of the losses are due to kinetic limitations at the catalyst surface. Since the exchange current density for hydrogen oxidation on Pt is three orders of magnitude higher than that for oxygen reduction on Pt, the activation losses at the cathode dominate the cell behaviour at low current densities. As the current density increases, the IR drop across each component of the

fuel cell increases and ohmic losses become significant. This is evident in the linear portion of the polarisation curve at intermediate current densities. At high current densities, mass transport effects dominate and the cell performance drops drastically. Transport of reactant gas through the pore structure of the backing layers and catalyst layers is the limiting factor here.

Polarisation curves provide information about the performance of the cell or stack as a whole. While they are a useful indicator of overall performance under service relevant conditions, they do not yield much information about the performance of individual components and are incapable of resolving time dependent processes occurring in the fuel cell. For this latter purpose current interrupt methods or impedance measurements are more commonly used. Polarisation curves are often converted to plots of power per unit area versus current density by multiplying the potential by the current density at each point on the curve.

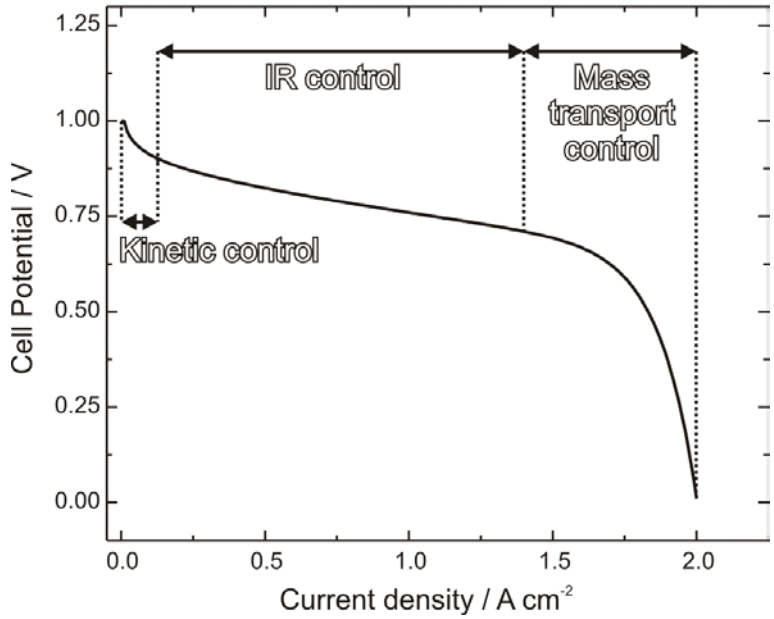

Figure 3.4 Typical polarisation curve for a PEMFC.

In studies of PEMFC cathodes it is important to keep the anode composition and loading constant if the anode is to be used as a reference electrode. The reversibility of the HOR on Pt is considered sufficient for this purpose, although when reformate is fed to the anode, the polarisation of both electrodes may be comparable. Voltammograms may be corrected for the IR drop across the membrane by measuring its high frequency resistance using current interrupt or impedance methods.

The electrochemical performance of a single electrode may be examined ex-situ by cyclic voltammetry (CV) and other common electrochemical techniques. Such half-cell experiments are carried out in a standard three electrode cell with an aqueous solution of acid (typically 0.5 M H_2SO_4) used to simulate the proton-conducting

electrolyte in a PEMFC. Half cell experiments are a convenient and relatively fast method of screening catalysts and comparing different MEA preparation techniques.

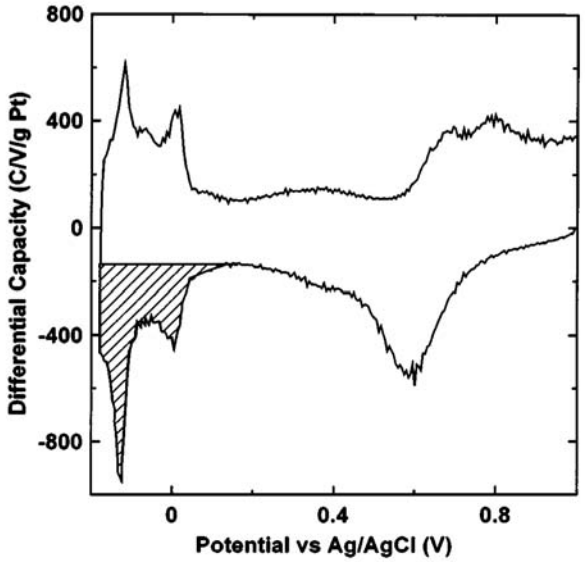

Figure 3.5 Illustration of the method used to calculate active surface area using hydrogen adsorption voltammetry[111]. The shaded area represents the charge due to hydrogen adsorption.

When the half cell experiment is carried out in solution purged with an inert gas such as nitrogen, integration of the hydrogen adsorption peak may be used to measure the active surface area of the catalyst. An example of such a voltammogram for a Pt catalyst is shown in Figure 3.5. The shaded area represents the total charge arising from hydrogen adsorption. The baseline is the capacitative current due to charging of the electrode double layer. This total charge may be converted to an active surface area (cm^2/g) using a proportionality constant, e.g. 210 $\mu C/cm^2$ for a platinum surface[112]. The Brunauer-Emmett-Teller (BET) method is used to calculate the effective surface area from nitrogen adsorption isotherms and is often quoted by manufacturers of catalysts. Ratios of active surface area to geometric surface area of order 10^3 are commonly obtained for PEMFC catalysts. Carbon monoxide stripping voltammetry is another common technique for determining the active surface area, operating under the same principle.

Many half-cell studies have focused on the oxygen reduction reaction (ORR) since it has a significantly larger overpotential on Pt than the hydrogen oxidation reaction (HOR). Kinetic parameters such as exchange current density and Tafel slope may be readily extracted from voltammograms obtained in O_2-saturated solution.

Cyclic voltammetry is the most common ex-situ diagnostic tool for probing the electrochemical activity of catalyst layers. Most PEMFC catalyst layers consist of a mixture of carbon-supported Pt and Nafion or Nafion-like ionomer. Most studies are divided between the determination of active area of the catalyst[113] and the elucidation

of the kinetics of the ORR at the triple phase boundary (TPB) between ionomer, catalyst and open pore[114]. The undesirable effects of poisons such as CO, which adsorb onto the catalyst surface thereby decreasing the number of available catalytic sites, have been well documented[115].

Stevens and Dahn compared the active surface area of a high surface area Pt/C catalyst (E-TEK BP2000, BET surface area 1300 m^2/g) to that of a lower surface area Pt/C catalyst (E-TEK XC72, BET surface area 270 m^2/g) as a function of Pt loading and particle size. The catalysts were mixed with 5% Nafion in a mixture of aliphatic alcohols, water and isopropanol and deposited on a glassy carbon electrode. Voltammograms were obtained in a three electrode cell containing 0.1 M HCO_4. An optimum Pt particle size of 2 nm was identified for both types of catalyst[116]. The XC72 samples showed a marked decrease in active surface area with increasing Pt loading, while no distinct trend was observed for the BP2000 samples.

Gloaguen et al used a rotating disk electrode (RDE) to allow correction of mass transport effects in solution[117]. The active layer consisted of 5% Nafion with 30 wt% Pt/Vulcan XC72 (E-TEK) and the electrolyte used for the CV experiments was 0.5 M H_2SO_4. Tafel plots for the ORR showed a double Tafel slope, with the slope at high potentials relevant to PEMFC operation close to 2.3RT/F. An exchange current density of 7×10^{-11} A/cm^2 was obtained at 20 °C and 1 atm pressure which compares well with that obtained for bulk platinum in various electrolytes. An optimum Pt particle size of 3.5 nm was identified in this study.

The kinetics of the ORR are governed by the amount of triple phase boundary in the active layer of the cathode. Due to the complexity of the heterogeneous structure of the active layer, the amount of TPB is difficult to determine. More detailed characterisation of the TPB in PEMFC active layers is required to understand the correlation between catalyst microstructure and performance. Pt microelectrodes have been used to study the ORR at solid state Pt/Nafion interfaces[118,119]. Recently O'Hayre and Prinz patterned circular Pt-catalyst microstructures on Nafion using a focused ion beam (FIB) system and investigated the ORR kinetics using impedance spectroscopy[120]. For electrodes smaller than 40 μm a direct relationship between electrode circumference and faradaic impedance was observed, indicating that the ORR kinetics scale with length of TPB. The authors proposed the use of a TPB width term in a coupled reaction/diffusion model to bridge the results of area-related and perimeter-related ORR kinetics.

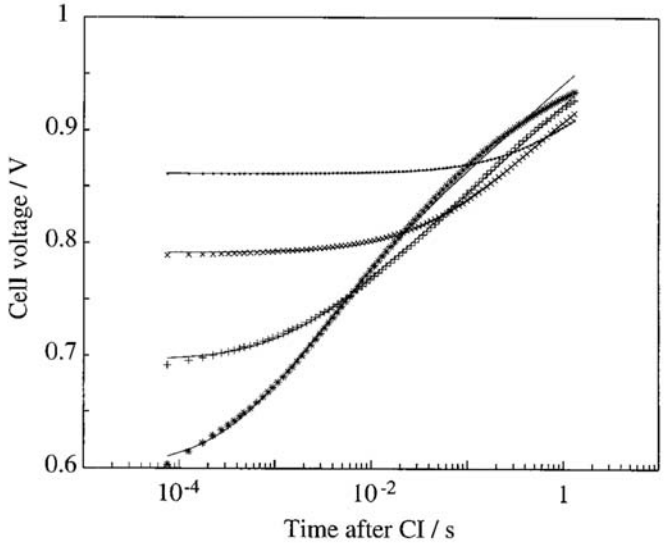

Figure 3.6 Relaxation curves of PEMFC voltage after current interruption for current densities of (.) 1, (x) 10, (+) 100 and (*) 400 mA/cm^2 before interruption[121].

Jaouen et al[122] recently applied the current interrupt technique to the characterisation of electrode performance in PEM fuel cells. The fuel cell is operated at a constant current before the measurement and a voltage transient is recorded upon interruption of the current. The ohmic losses disappear almost immediately and the electrochemical overpotentials decay to the open circuit value over a longer timescale. They found that analysis of the voltage relaxation curve after the disappearance of the ohmic losses could yield information on the electrochemical performance of the electrodes. An example of relaxation curves at a number of different current densities is shown in Figure 3.6. The plateau at short times is indicative of O_2 diffusion limitation, while limitation by proton migration results in no plateau at short times and a transition to a Tafel slope at longer times. A model containing expressions for Tafel kinetics, oxygen diffusion in agglomerates, proton migration and double layer capacitance was developed[123], which fitted the experimental data well up to a current density of 200 mA/cm^2.

Impedance spectroscopy is a powerful tool for the analysis of electrochemical systems. In contrast to linear sweep and potential step methods, where the system is perturbed far from equilibrium, a small ac voltage perturbation is applied to the cell and the amplitude and phase of the resulting signal are measured as a function of frequency. This allows the resolution of dynamic processes occurring on different timescales in the system being studied.

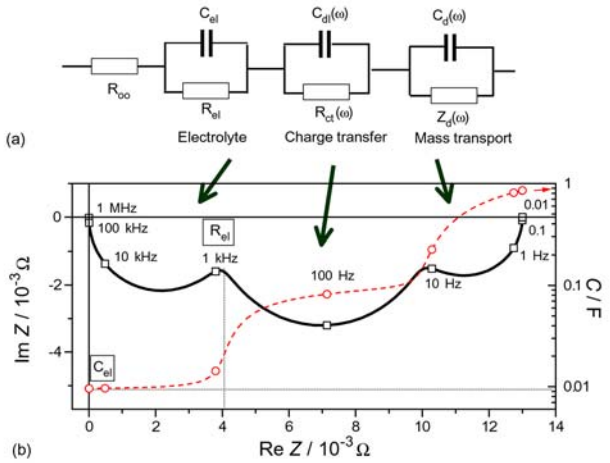

Figure 3.7 (a) General equivalent circuit for a PEMFC (b) Schematic frequency response of impedance and capacitance[124].

Impedance spectra are conventionally plotted in both Bode and Nyquist form. In a Bode plot, the amplitude and phase of the impedance is plotted as a function of frequency, while in a Nyquist plot the imaginary part of the impedance is plotted against the real part at each frequency. A typical Nyquist plot for a PEMFC consists of three depressed semicircles as shown in Figure 3.7, where the frequency increases from right to left. The major axis of the high frequency arc is proportional to the ohmic resistance of the membrane, which can be directly compared to that obtained from current interrupt measurements. The major axis of the second arc is a measure of the charge transfer resistance of the electrochemical reaction, which is usually dominated by the impedance of the cathode. The low frequency arc reflects the impedance due to mass transport limitations, which is dominated by the porous layers.

The measurement of the magnitude and phase of the impedance as a function of frequency may be readily analysed in terms of equivalent circuits. In this type of analysis, the cell response is modelled on that of an electrical circuit containing combinations of resistors and capacitors, each representing a particular physical or chemical process. In general, a resistor represents a conductive path, such as ion migration in electrolyte or the charge transfer accompanying an electrode reaction. A capacitor represents a space charge layer, such as the electrical double layer at the electrode/electrolyte interface. Mass transport phenomena, such as diffusion to an electrode surface, are represented by a Warburg impedance, which is manifested in a straight line with a slope of unity in the Nyquist plot at low frequencies. A constant phase element (CPE), a non-intuitive circuit element that has no analogue in conventional electronics, was invented to describe the behaviour of non-ideal surfaces. The phase of the CPE is independent of frequency and represents a distribution of time constants due to the inhomogeneity of the surface. The CPE may be represented by a network of RC-circuits with time constants spanning orders of magnitude and may be modelled by fractal geometry.

4 KEY ISSUES

The development of test methods and protocols for evaluation and quality control of catalysts and electrodes is a key goal for the fuel cell industry. At present, reliable evaluation of catalyst performance requires the catalyst to be fully incorporated in the MEA, as ex-situ electrochemical tests are often not representative of in-situ performance. This is because catalyst activity is strongly dependent on the processing technique used. In-situ testing is time consuming and expensive and can itself generate variable data due to differences in cell construction and conditioning. It is essential to develop faster and cheaper test methods, which remain representative of performance in a real fuel cell. A large number of tests is desirable to smooth out statistical variations, which requires high-throughput or combinatorial techniques.

Standard electrochemical techniques such as voltammetry and impedance spectroscopy would appear to be the most straightforward way to evaluate catalyst performance. The key issue is the appropriate arrangement of the catalyst on the substrate so that a representative test of in-situ performance is obtained. The simplest arrangement would probably be the deposition of the metal particles on a glassy carbon electrode. However, it is likely that some ionomer would need to be incorporated into the electrode in order to mimic the three phase boundary. The addition of a hydrophobic agent such as PTFE may also be required. An ideal test system would allow a large number of catalysts to be tested at once. This could be achieved by an electrode array, produced by screen printing. For combinatorial testing, a compositional gradient across the electrode could be introduced and individual segments of the electrode could be isolated using a mask.

A key requirement in the development of such ex-situ tests is to ensure that the comparison with in-situ performance is valid. Hence it will be important to perform in-situ testing simultaneously in order to validate this perspective. The effectiveness of impedance spectroscopy in the evaluation of catalyst performance should also be investigated.

Chan et al[125] recently evaluated a number of high-throughput electrochemical techniques for characterising fuel cell catalysts. They found that while an optical fluorescence technique could distinguish active and inactive catalysts, it could not rank them accurately. A 25-electrode array fuel cell technique produced better agreement with in-situ performance than disk electrode linear sweep voltammetry. It was proposed that the optical technique could be used as an initial screening process, with t more precise technique used to qualify the results. The authors noted that a wide range of performance was obtained for catalysts of the same nominal composition but differing preparation methods.

Koponen et al[126] have developed a jet impingement technique for characterising catalyst inks and catalyst layers using cyclic voltammetry. They showed that the active surface area of the catalyst was proportional to the mass density of Pt in the catalyst layers. The half cell arrangement shown in Figure 4.1 was used to test cathode catalyst layers in the presence of O_2.

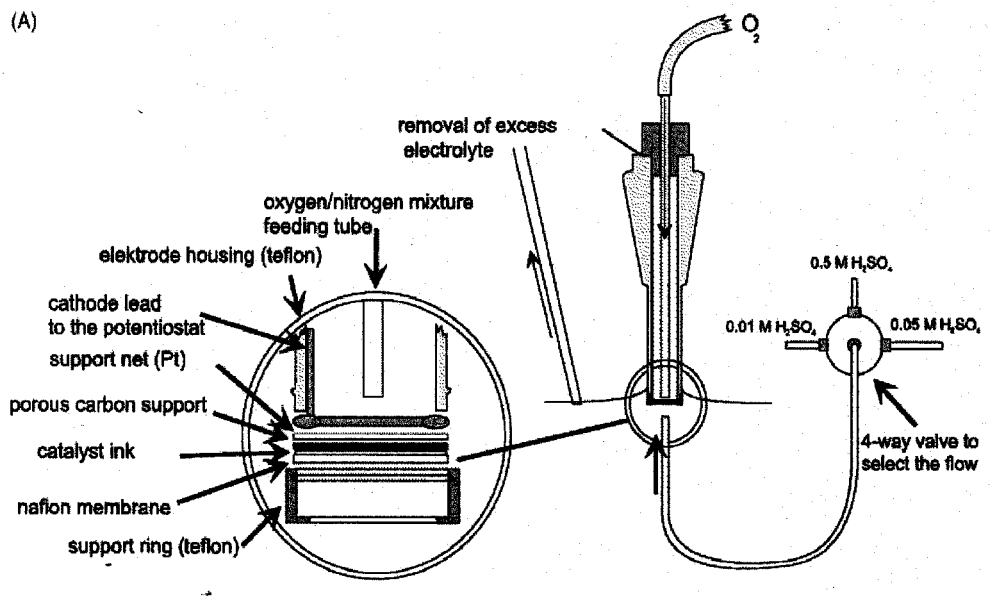

Figure 4.1 Measuring device for half cell characterisation of cathode catalyst layers[127].

In addition to macroscale measurements on catalysts and electrodes, the development of techniques to improve understanding of processes on the nanoscale is critical. While physical and chemical characterisation techniques for catalytic materials (e.g. electron microscopy, XRD, XPS) are relatively well established, there is a clear need to develop measurement techniques to probe the reactivity of surfaces on the micro- to nanoscale. There are a number of scanning probe techniques which could be applied to appropriate model systems. The use of scanning probe techniques for nanoscale characterisation is limited to very smooth surfaces, which prohibits their application to real world catalyst systems. However, a progression towards model systems that increasingly mimic real world catalysts would seem achievable. Three likely candidate techniques are:

1. Electrochemical atomic force microscopy (E-AFM)
2. Scanning electrochemical microscopy (SECM)
3. Scanning vibrating probe (SVP)

NPL has expertise in all three techniques. An overview of scanning probe techniques together with recommendations for future research at NPL was published recently by Turnbull[128]. E-AFM is a modification of AFM, allowing the profiling of a surface to take place in the liquid phase and under potential control. Its use is therefore limited to relatively smooth surfaces. However, SECM and SVP techniques could bridge the gap between microscale and nanoscale characterisation, providing that probes with sufficiently small tips can be obtained or manufactured. The SECM measures the current at an ultramicroelectrode (UME) placed in the vicinity of a substrate. The presence of the substrate perturbs the electrochemical response of the UME, yielding

information about the local reactivity of the surface. The SVP measures the potential drop generated by current flow in a small volume of solution by vibrating PtIr-tipped microelectrodes between two fixed points in the electrolyte at a defined distance from the surface. The SECM is more versatile than the SVP and can be operated in several different modes in order to visualise lateral variations in surface activity[129]. The feedback mode, illustrated in Figure 4.2, is the most potentially useful mode for the study of heterogeneous catalysis.

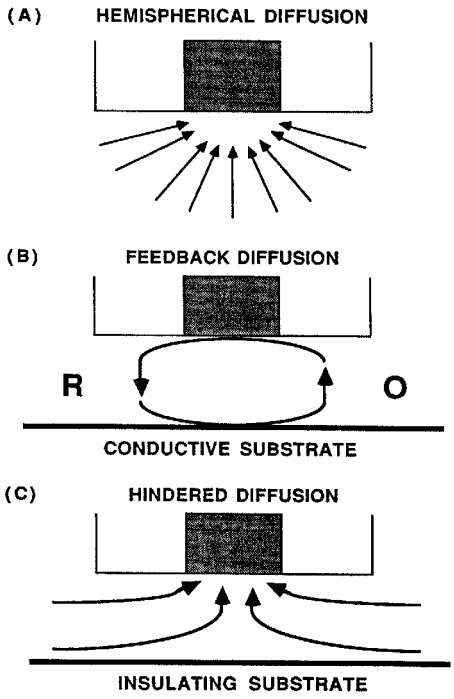

Figure 4.2 Principle of SECM operation in feedback mode far from substrate (A) and close to conducting (B) and insulating (C) substrates[130].

Depending on the surface roughness of the substrate, a compromise on insulating sheath diameter is required in feedback mode. A large sheath to tip diameter ratio is generally preferable to increase the contrast between active and inactive regions of the surface, but there is an accompanying risk of damage due to collision with the surface. This is a particular problem for rough surfaces such as fuel cell electrodes. It is envisaged that a modified-AFM tip could be used to achieve the optimum resolution. The application of SECM and SVP techniques to catalyst systems presents a significant challenge. Nevertheless, such studies would at the very least provide an assessment of the limitations of these techniques when applied to nanoparticulate systems. The use of SECM could provide insight into the scale of the clustering of catalyst particles. The electrochemical profiling of a surface on the microscale would then provide guidance as to the specific location of E-AFM studies.

The move towards smaller and smaller tip sizes will enable characterisation of catalytic surfaces at decreasing length scales. AFM tips modified with carbon

nanotubes are attracting interest as their small diameter and high aspect ratio dramatically increase image resolution[131]. In addition, their excellent mechanical properties prevent breakage and wear. However, when such a tip is immersed in solution, the nanotube is quickly lost due to acoustic vibration. This can be rectified by using the nanotube as a template and applying a metal coating to provide mechanical support.

It is essential that the electrochemical techniques discussed above are backed up by physical characterisation of the catalyst. The detailed mechanism of catalyst operation is not well understood. Issues remaining to be resolved include particle size effects, the effect of the metal-support interaction and alloy formation/oxidation. An important aspect of fuel cell research is the correlation between structural characterisation and catalytic performance. A wide range of measurement techniques is available for the characterisation of particle size, surface area, density, porosity, physisorption and chemisorption in catalyst materials. The establishment of such facilities would bridge a significant gap in NPL's materials characterisation capabilities and would provide valuable support for related work on fuel cells.

A review of the challenges in the structural characterisation of nanodispersed catalytic materials was recently published by Roth et al[132]. They emphasised that only a combination of microscopy, spectroscopy and diffraction can ensure accurate structural characterisation since most techniques are operating close to their limits of resolution. They also recommended increased use of in-situ techniques, particularly in monitoring degradation.

5 CONCLUSIONS

- The development of representative test protocols for ex-situ characterisation of catalysts would provide significant cost and time savings to the fuel cell industry.

- An assessment of the suitability of electrochemical testing of simple model electrodes would be a first step towards the establishment of a test protocol.

- The application of scanning probe techniques to the study of catalytic behaviour on the micro- to nanoscale would advance fundamental understanding of the underpinning science, allowing manufacturers to reduce costs and improve performance.

- Physical characterisation of the catalyst is essential to support electrochemical characterisation techniques. The establishment of such facilities would bridge a significant gap in NPL's materials characterisation capabilities.

6 ACKNOWLEDGEMENTS

This work was conducted as part of the Materials Processing programme, a joint venture between the United Kingdom Department of Trade and Industry and an Industrial Advisory Group comprising C Tech Innovation, Ceres Power, CMR Fuel Cells, Dart Sensors, Gary Acres, Ineos Chlor, Intelligent Energy, Johnson Matthey, Rolls Royce Fuel Cells, Solartron Analytical, Imperial College and the University of Birmingham.

7 REFERENCES

[1] Reprinted from D.M. Bernardi, M.W. Verbrugge, Proc. of the Symposium on Modeling of Batteries and Fuel Cells, 1991, Phoenix, U.S.A., p.240. Copyright 1991, The Electrochemical Society.

[2] S.K.A. Wasmus, J. Electroanal. Chem., **461**, 14 (1999).

[3] Reprinted from J.H. Tian, F.B. Wang, Z.Q. Shan, R.J. Wang, J.Y. Zhang, J. Appl. Electrochem., **34**, 461, 2004 with permission from Kluwer.

[4] E. Auer, A. Freund, J. Pietsch, T. Tacke, Appl. Catal. A **173**, 259 (1998).

[5] E. Antolini, J. Mater. Sci., **38**, 2995 (2003).

[6] E. Czaran, J. Finster, K.H. Schnabel, Z. Anorg. Allg. Chem., **443**, 175 (1978).

[7] S.R. De Miguel, O.A. Scelza, M.C. Roman-Martinez, C. Salinas-Martinez, D. Cazorla-Amoros, A. Linares-Solano, Appl. Catal. A **170**, 93 (1998).

[8] F. Coloma, A. Sepulveda-Escribano, J.L. Fierro, F. Rodriguez-Reinoso, Langmuir, **10**, 750 (1994).

[9] M.A. Fraga, E. Jordao, M.J. Mendes, M.M.A. Freitas, J.L. Faria, J.L. Figuerido, J. Catal, **209**, 355 (2002).

[10] H.E. van Dam, H. van Bekkum, J. Catal., **131**, 335 (1991).

[11] G.C. Torres, E.I. Iablonski, G.T. Baronetti, A.A. Castro, S.R. De Miguel, O.A. Scelza, M.D. Blanco, M.A. Pena Jimenez, J.L.G. Fierro, Appl. Catal. A, **161**, 213 (1997).

[12] S.S. Barton, M.J.B. Evans, E. Halliop, J.A.F. Macdonald, Carbon, **35**, 1361 (1997).

[13] C. Leon, Y. Leon, J.M. Solar, V. Calemma, L.R. Radovic, Carbon, **30**, 797 (1992).

[14] J.F. Lambert, M. Che, J. Mol. Catal. A, **162**, 5 (2000).

[15] S.R. Miguel, O.A. Scelza, M.C. Roman-Martinez, C.S.M. Lecea, D. Cazorla-Amoros, A. Linares-Solano, Appl. Catal. A, **170**, 93 (1998).

[16] L.D. Ageeva, N.A. Kolpakova, T.V Kovyrkyna, N.P Potsyapun, N.S. Buinovskii, J. Anal. Chem., **56**, 137 (2001).

[17] Reprinted from E. Antolini, J. Mater. Sci., **38**, 2995 (2003).

[18] G.C. Torres, E.I. Iablonski, G.T. Baronetti, A.A. Castro, S.R. De Miguel, O.A. Scelza, M.D. Blanco, M.A. Pena Jimenez, J.L.G. Fierro, Appl. Catal. A, **161**, 213 (1997).

[19] C. Prado-Burguete, A. Linares-Solano, F. Rodriguez-Reinoso, C.S.M. Lecea, J. Catal, **115**, 98 (1989).

[20] D.J. Suh, T.J. Park, S.K. Ihm, Carbon, **31**, 427 (1993).

[21] A. Sepulveda-Escribano, F. Coloma, F. Rodriguez-Reinoso, Appl. Catal. A, **173**, 247 (1998).

[22] P. Ehrburger, O.P. Majahan, P.L.J. Walker, J. Catal., **43**, 61 (1974).

[23] F. Coloma, A. Sepulveda-Escribano, J.L. Fierro, F. Rodriguez-Reinoso, Langmuir, **10**, 750 (1994).

[24] A. Guerriero-Ruiz, P. Badenes, I. Rodriguez-Ramos, Appl. Catal. A, **173**, 313 (1998).

[25] M.A. Fraga, E. Jordao, M.J. Mendes, M.M.A. Freitas, J.L. Faria, J.L. Figuerido, J. Catal, **209**, 355 (2002).

[26] F. Yuan, G. Sasikumar, H. Ryu, J. New Materials Electrochem. Systems, 7, 311 (2004).

[27] Z. Liu, X. Lin, J.Y. Lee, W. Zhang, M. Han, L.M. Gan, Langmuir, **18**, 4054 (2002).
[28] E. Antolini, L. Giorgi, F. Cardellini, E. Passalacqua, J. Solid State Electrochem., **5**, 131 (2001).
[29] M. Uchida, Y. Aoyama, M. Tanabe, N. Yanagihara, N. Eda, A. Ohta, J. Electrochem. Soc., **142**, 2572 (1995).
[30] M. Watanabe, H. Sei, P. Stonehart, J. Electroanal. Chem., **261**, 375 (1989).
[31] M.A. Fraga, E. Jordao, M.J. Mendes, M.M.A. Freitas, J.L. Faria, J.L. Figuerido, J. Catal, **209**, 355 (2002).
[32] Reprinted from M. Uchida, Y. Aoyama, M. Tanabe, N. Yanagihara, N. Eda, A. Ohta, J. Electrochem. Soc., **142**, 2572 (1995).
[33] A. Honji, T. Mori, K. Tamura, Y. Hishinuma, J. Electrochem. Soc., **137**, 2084 (1990).
[34] X. Wang, I.M. Hsing, Electrochim. Acta, **47**, 2981 (2002).
[35] Reprinted from A. Honji, T. Mori, K. Tamura, Y. Hishinuma, J. Electrochem. Soc., **137**, 2084 (1990).
[36] Reprinted from A. Honji, T. Mori, K. Tamura, Y. Hishinuma, J. Electrochem. Soc., **137**, 2084 (1990).
[37] T. Yoshitake, Y. Shimakawa, S. Kuroshima, H. Kimura, T. Ichihashi, Y. Kubo, D. Kasuya, K. Takahashi, F. Kokai, M. Yudasaka, S. Iijima, Physica B, **323**, 124 (2002).
[38] H. Kim, P. Kim, Y. Park, J. Lee, K. Choi, J. Yi, Key Engineering Materials, **277-9**, 899 (2005).
[39] E.G. Franco, E. Arico, M. Linardi, C. Roth, N. Martz, H. Fuess, Mat. Sci. For., **416-8**, 4 (2003).
[40] J.H. Tian, F.B. Wang, Z.Q. Shan, R.J. Wang, J.Y. Zhang, J. Appl. Electrochem., **34**, 461 (2004).
[41] A. Stoyonova, V. Naidenov, K. Petrov, I. Nikolov, T. Vitanov, E. Budevski, J. Appl. Electrochem., **29**, 1197 (1999).
[42] E. Antolini, F. Cardellini, E. Giacometti, G. Squadrito, J. Mater. Sci., **37**, 133 (2002).
[43] T. Torre, A.S. Arico, V. Alderucci, V. Antonucci, N. Giordano, Appl. Catal. A, **114**, 257 (1994).
[44] V.M. Jalan, in 'Extended Abstracts, Meeting Electrochemical Society', Montreal, Canada, 1982.
[45] E. Antolini, F. Cardellini, E. Giacometti, G. Squadrito, J. Mater. Sci., **37**, 133 (2002).
[46] S.C. Roy, P.A. Christensen, A. Hamnett, K.M. Thomas, V. Trapp, J. Electrochem. Soc., **143**, 3073 (1996).
[47] T. Torre, A.S. Arico, V. Alderucci, V. Antonucci, N. Giordano, Appl. Catal. A, **114**, 257 (1994).
[48] Reprinted from E. Antolini, F. Cardellini, E. Giacometti, G. Squadrito, J. Mater. Sci., **37**, 133 (2002).
[49] S. Mukerjee, S. Srinivasan, M.P. Soriaga, J. McBreen, J. Electrochem. Soc., **142**, 1409 (1995).
[50] K. Kinoshita, J. Electrochem. Soc., **137**, 845 (1990).
[51] W. Romanowski, Surf. Sci., **18**, 373 (1969).
[52] M.L. Stattler, P.N. Ross, Ultramicroscopy, **20** , 21 (1986).

[53] M. Komiyama, J. Kobayashi, S. Morica, J. Vac. Sci. Tech., **8**, 608 (1990).
[54] Reprinted from K. Kinoshita, J. Electrochem. Soc., **137**, 845 (1990).
[55] Reprinted from E. Antolini, J. Appl. Electrochem., **34**, 563 (2004).
[56] E. Antolini, J. Appl. Electrochem., **34**, 563 (2004).
[57] P. Staiti, Z. Poltarewski, V. Alderucci, N. Giordano, Int. J. Hydrogen Energy, **19**, 254 (1994).
[58] E. Passalacqua, F. Lufrano, G. Squadrito, A. Patti, L. Giorgi, Electrochim. Acta, **46**, 799 (2001).
[59] V.A. Paganin, E.A. Ticianelli, E.R. Gonzalez, J. Appl. Electrochem., **26**, 297 (1996).
[60] D.H. Peck, Y.G. Chun, C.S. Kim, D.H. Jun, D.R. Shin, J. New Mat. Electrochem. Systems, **2**, 121 (1999).
[61] J.M. Song, S.Y. Cha, W.M. Lee, J. Power Sources, **94**, 78 (2001).
[62] S.J. Lee, S. Mukerjee, J. McBreen, Y.W. Rho, Y.T. Kho, T.H. Lee, Electrochim. Acta, **42**, 3693 (1998).
[63] A. Fischer, H. Wendt, Proc. Fuel Cell Seminar 1996, Orlando, U.S.A., p. 579.
[64] M. Uchida, Y. Aoyama, N. Eda, A. Ohta, J. Electrochem. Soc., **142**, 4143 (1995).
[65] N. Jia, R.B. Martin, Z. Qi, M.C. Lefebvre, P.G. Pickup, Electrochim. Acta, **43**, 3665 (2001).
[66] Y.G. Chun, C.S. Kim, D.H. Peck, D.R. Shin, J. Power Sources, **71**, 174 (1998).
[67] A. Fischer, J. Jindra, H. Wendt, J. Applied Electrochem., **28**, 277 (1998).
[68] M.S. Wilson, S. Gottesfeld, J. Electrochem. Soc., **139**, L28 (1992).
[69] M.S. Wilson, S. Gottesfeld, J. Applied Electrochem., **22**, 1 (1992).
[70] A. Fischer, J. Jindra, H. Wendt, J. Applied Electrochem., **28**, 277 (1998).
[71] P.A. Webb, C. Orr, Analytical Methods in Fine Particle Technology, Micrometrics Instrument Corporation, p. 155, 1997.
[72] M. Watanabe, M. Tomikawa, S. Motoo, J. Electroanal. Chem., **195**, 81 (1985).
[73] M. Uchida, Y. Aoyama, N. Eda, A. Ohta, J. Electrochem. Soc., **142**, 4143 (1995).
[74] M. Uchida, Y. Fukuoka, Y. Sugawara, N. Eda, A. Ohta, Proc. Fuel Cell Seminar 1996, Orlando, U.S.A., p. 612.
[75] A. Lundblad, J. New Mat. Electrochem. Systems, **7**, 21-28 (2004).
[76] S. Gamburzev, A.J. Appleby, J. Power Sources, **107**, 5 (2002).
[77] P. Gode, F. Jaouen, G. Lindbergh, A. Lundblad, G. Sundholm, Electrochim. Acta, **48**, 4175 (2003).
[78] F. Jaouen, G. Lindbergh, G. Sundholm, J. Electrochem. Soc., **149**, A437 (2002).
[79] Reprinted from P. Gode, F. Jaouen, G. Lindbergh, A. Lundblad, G. Sundholm, Electrochim. Acta, **48**, 4175 (2003).
[80] F. Lufrano, E. Passalacqua, G. Squadrito, A. Patti, L. Giorgi, J. Appl. Electrochem., **29**, 445 (1999).
[81] J.M. Song, S.Y. Cha, W.M. Lee, J. Power Sources, 94, 78 (2001).
[82] E. Antolini, A. Pozio, L. Giorgi, E. Passalacqua, Electrochim. Acta, **43**, 3675 (1998).
[83] Reprinted from E. Passalacqua, G. Squadrito, F. Lufrano, A. Patti, L. Giorgi, J. Appl. Electrochem., **31**, 449 (2001).
[84] E. Passalacqua, G. Squadrito, F. Lufrano, A. Patti, L. Giorgi, J. Appl. Electrochem., **31**, 449 (2001).
[85] C.S. Kong, D.Y. Kim, H.K. Lee, Y.G. Shul, T.H. Lee, J. Power Sources, 108, 185 (2002).

[86] M. Neergat, A.K. Shukla, J. Power Sources, **104**, 289 (2002).
[87] J. Moreira, A.L. Ocampo, P.J. Sebastian, M.A. Smit, M.D. Salazar, P. del Angel, J.A. Montoya, R. Perez, L. Martinez, Int. J. Hydrogen Energy, **28**, 625 (2003).
[88] Y.S. Hsu, C.S. Hsu, Y.C. Cheng, Proc. 3rd International Fuel Cell Conference, Nagoya, Japan, 1999, p. 503.
[89] Z. Poltarewski, P. Staiti, V. Alderucci, W. Wieczarek, N. Giordano, J. Electrochem. Soc., **139**, 761 (1992).
[90] Z. Qi, A. Kaufman, J. Power Sources, **113**, 37 (2003).
[91] G. Li, P.G. Pickup, J. Electrochem. Soc., **150**, C745 (2003).
[92] M. Uchida, Y. Aoyama, N. Eda, A. Ohta, J. Electrochem. Soc., **142**, 4143 (1995).
[93] E. Passalacqua, F. Lufrano, G. Squadrito, A. Patti, L. Giorgi, Electrochim. Acta, **46**, 799 (2001).
[94] V. Paganin, E.A. Ticianelli, E.R. Gonzalez, J. Appl. Electrochem., 26, 297 (1996).
[95] E. Antolini, L. Giorgi, A. Pozio, E. Passalacqua, J. Power Sources, **77**, 136 (1999).
[96] E. Antolini, R.R. Passos, E.A. Ticianelli, J. Appl. Electrochem., **32**, 383 (2002).
[97] E. Antolini, R.R. Passos, E.A. Ticianelli, J. Power Sources., **109**, 477 (2002).
[98] J.H. Kim, H.Y. Ha, I.H. Oh, S.A. Hong, H.I. Lee, J. Power Sources, **135**, 29 (2004).
[99] T.H. Yang, Y.G. Yoon, G.G. Park, W.Y. Lee, C.S. Kim, J. Power Sources, **127**, 230 (2004).
[100] H.A. Abaoud, M. Ghouse, K.V. Lovell, G.N. Al-Motiary, Journal of New Materials for Electrochemical Systems, **6**, 149 (2003).
[101] Mustafa, H. Usui, I. Shige, H. Suzuki, T. Kobayashi, Y. Miyazaki, T. Ioroi, K. Yasuda, J. Chemical Engineering Japan, **37**, 31 (2004).
[102] M.S. Loffler, B. Gross, H. Natter, R. Hemplemann, T. Krajewski, J. Divisek, Scripta Mater., **44**, 2253 (2001).
[103] H. Kim, B.N. Popov, Electrochem. Solid State Letters, **7**, A71 (2004).
[104] K. Hayashi, N. Furuya, J. Electrochem. Soc., **151**, A354 (2004).
[105] T. Frey, K.A. Friedrich, L. Jorissen, J. Garche, J. Electrochem. Soc., 152, A545 (2005).
[106] E. Gulzow, M. Schulze, N. Wagner, T. Kaz, R. Reissner, G. Steinhilber, A. Schneider, J. Power Sources, **86**, 352 (2000).
[107] S.E. Foster, P.J. Mitchell, R.J. Mortimer, P.L. Adcock, 19th International Power Sources Symposium, Brighton, UK, 1995, p. 407.
[108] M. Pan, H. Tang, S.P. Jiang, Z. Liu, J. Electrochem. Soc., **152**, A1081 (2005).
[109] M. Prasanna, H.Y. Ha, E.A. Cho, S.-A. Hong, I.-H. Oh, J. Power Sources, 131, 147 (2004).
[110] H.-S. Chu, C. Yeh, F. Chen, J. Power Sources, **123**, 1 (2003).
[111] Reprinted from D.A. Stevens, J.R. Dahn, J. Electrochem. Soc., **150**, A770 (2003).
[112] T. Biegler, D.A.J. Rand, R. Woods, J. Electroanal. Chem., **29**, 269 (1971).
[113] A. Essalik, K. Amouzegar, O. Savadogo, J. Appl. Electrochem., **25**, 404 (1995).
[114] A. Parthasarathay, S. Srinivasan, A.J. Appleby, C.R. Martin, J. Electroanal. Chem., **339**, 101 (1992).
[115] H. Gasteiger, N. Markovic, P.N. Ross, J. Phys. Chem., **99**, 8290 (1995).
[116] D.A. Stevens, J.R. Dahn, J. Electrochem. Soc., **150**, A770 (2003).
[117] F. Gloaguen, F. Andolfatto, R. Durand, P. Ozil, J. Appl. Electrochem., 24, 863 (1994).

[118] A. Parthasarathay, C.R. Martin, S. Srinivasan, J. Electrochem. Soc., **138**, 916 (1991).
[119] F. Uribe, T.E. Springer, S. Gottesfeld, J. Electrochem. Soc., **139**, 765 (1992).
[120] R. O'Hayre, F.B. Prinz, J. Electrochem. Soc., **151**, A756 (2004).
[121] Reprinted from F. Jaouen, G. Lindbergh, J. Electrochem. Soc., **150**, A1711 (2003).
[122] F. Jaouen, G. Lindbergh, J. Electrochem. Soc., **150**, A1711 (2003).
[123] F. Jaouen, G. Lindbergh, J. Electrochem. Soc., **150**, A1699 (2003).
[124] Reprinted from P. Kurzweil, H.-J. Fischle, J. Power Sources, **127**, 331 (2004).
[125] B.C. Chan, R. Liu, K. Jambunathan, H. Zhang, G. Chen, T.E. Mallouk, E.S. Smotkin, J. Electrochem. Soc., **152**, A594 (2005).
[126] U. Koponen, H. Kumpulainen, M. Begelin, J. Keskinen, T. Peltonen, V. Valkiainen, M. Wasberg, J. Power Sources, **118**, 325 (2003).
[127] Reprinted from U. Koponen, H. Kumpulainen, M. Begelin, J. Keskinen, T. Peltonen, V. Valkiainen, M. Wasberg, J. Power Sources, **118**, 325 (2003).
[128] A. Turnbull, NPL Report DEPC MPE 011, March 2005.
[129] A.J. Bard, M.V. Mirkin (Eds.), Scanning Electrochemical Microscopy, Marcel Dekker, New York, 2001.
[130] Reprinted from A.J. Bard, M.V. Mirkin (Eds.), Scanning Electrochemical Microscopy, Marcel Dekker, New York, 2001.
[131] H. Dai, J.H. Hafner, A.G. Rinzler, D.T. Colbert, R.E. Smalley, Nature, **384**, 147 (1996).
[132] C. Roth, N. Martz, H. Fuess, Journal of New Materials for Electrochemical Systems, **7**, 117 (2004).